ISSN 3048-8222 (Online) | www.ijsate.com | editor@ijsate.com

International Journal of
Science, Architecture, Technology and Environment

Application of the Extended Kalman Filter in Motion State Estimation Using a New-Generation Inertial Sensor

Nguyen Ha Giang[1]

[1]Missile Faculty, Air Defence-Air Force Academy, Ha Noi, Viet Nam

*Corresponding author email: bopbopbaby88@gmail.com

DOI: https://doi.org/10.63680/ijsate0726003.3

Abstract

This paper presents a method for evaluating the performance of the Extended Kalman Filter (EKF) in estimating the motion states of ships operating in dynamic ocean wave conditions using the new-generation inertial sensor Xsens MTi-600. A six-degree-of-freedom dynamic model of the ship is constructed, taking into account the influence of random wave disturbances, sensor bias drift, and acceleration measurement noise. The EKF algorithm is designed to fuse information from gyroscopes and accelerometers in order to accurately estimate roll, pitch, and yaw angles and to correct bias errors over time. Simulation results show that EKF effectively compensates for sensor drift, significantly reduces high-frequency noise, and closely tracks the true state values even under strong wave oscillations. The evaluation results of the error spectra and attitude angles demonstrate that EKF operates stably and is well suited for orientation and stabilization applications of marine observation platforms.

Keywords: Extended Kalman Filter, MEMS inertial sensor, state estimation, ship motion, Euler angles, random wave spectrum.

1. Introduction

In modern ship control and navigation systems, accurate estimation of motion states plays a crucial role in ensuring safety and operational efficiency. However, under severe sea conditions, the measurement signals from inertial sensors (IMU) are often significantly affected by random noise, drift errors, and nonlinear dynamics, leading to degradation of the accuracy of direct measurements. To overcome this problem, nonlinear filters such as the EKF have been widely applied to integrate information from sensors and system dynamics models, thereby providing optimal state estimation in noisy environments. However, the actual performance of EKF depends greatly on the sensor model, the wave spectral characteristics, and the structure of the measurement noise matrix.

This paper focuses on constructing a complete simulation model of the sea wave environment based on the JONSWAP spectrum, simulating the inertial sensor Xsens MTi-600 with realistic errors, and implementing the EKF algorithm to estimate the ship's motion angles (roll and pitch). The simulation results are compared with the traditional complementary filter method to quantitatively evaluate the effectiveness of EKF under Beaufort sea state 6 conditions. The research aims toward practical applications in orientation stabilization and automatic control systems for ships operating in dynamic seas.

ISSN 3048-8222 (Online) | www.ijsate.com | editor@ijsate.com

2. Algorithm Synthesis

To accurately estimate the roll–pitch–yaw angles of a ship operating under dynamic sea wave conditions, the EKF is applied to the nonlinear Euler angle kinematic model, combined with gyro bias compensation. The system state is represented as a six-dimensional vector:

$$\boldsymbol{x}(t) = \begin{bmatrix} \phi(k) & \theta(t) & \psi(t) & b_p(t) & b_q(t) & b_r(t) \end{bmatrix}^T \tag{1}$$

Where:

ϕ, θ, ψ : roll–pitch–yaw angles (deg);

b_p, b_q, b_r : gyro bias on each axis (deg/s).

The Euler angle kinematics are described by the nonlinear relationship between the measured angular velocity and the derivatives of the Euler angles. The general form of the state model is:

$$\dot{\boldsymbol{x}}(t) = \boldsymbol{f}(\boldsymbol{x}(t), \boldsymbol{u}(t)) + \mathbf{w}(t) \tag{2}$$

Where:

$\boldsymbol{u}(t) = [\mathrm{p}_m(\mathrm{t}), \mathrm{q}_m(\mathrm{t}), \mathrm{r}_m(\mathrm{t})]^T$ is the measured angular velocity signal from the gyroscope;

p_m, q_m, r_m are the measured angular velocities from the IMU [deg/s];

$\mathbf{w}(t)$ is the process noise with covariance $\boldsymbol{Q}$.

The nonlinear dynamic model of $\boldsymbol{x}(t)$ is determined according to the Euler–Body kinematic relationship:

$$\dot{\phi} = (p_m - b_p) + (q_m - b_q)\sin\phi\tan\theta + (r_m - b_r)\cos\phi\tan\theta \tag{3}$$

$$\dot{\theta} = (q_m - b_q)\cos\phi - (r_m - b_r)\sin\phi \tag{4}$$

$$\dot{\psi} = (q_m - b_q)\frac{\sin\phi}{\cos\theta} + (r_m - b_r)\frac{\cos\phi}{\cos\theta} \tag{5}$$

$$\dot{b}_p = 0, \dot{b}_q = 0, \dot{b}_r = 0 \tag{6}$$

The bias drift is modeled as a random walk process (the derivatives are assumed zero in the mean model).

Discretizing equations (3)–(6) with sampling period T_S ta được:

$$\boldsymbol{x}_{k|k-1} = \boldsymbol{x}_{k-1} + T_S \boldsymbol{f}(\boldsymbol{x}_{k-1}, \boldsymbol{u}_{k-1}) \tag{7}$$

At each step, EKF uses the Jacobian matrix $\boldsymbol{F}_k$ to linearly approximate the nonlinear function (3)–(6) around the current estimate:

$$\boldsymbol{F}_k = \left.\frac{\partial \boldsymbol{f}}{\partial \boldsymbol{x}}\right|_{\boldsymbol{x}_{k-1}, \boldsymbol{u}_{k-1}} \tag{8}$$

$\boldsymbol{F}_k$ is the Jacobian matrix:

$$\boldsymbol{F}_k = \begin{bmatrix} F_{11} & F_{12} & 0 & -1 & F_{15} & F_{16} \\ F_{21} & 0 & 0 & 0 & F_{25} & F_{26} \\ F_{31} & 0 & 0 & F_{34} & F_{35} & F_{36} \\ 0 & 0 & 0 & 0 & 0 & 0 \\ 0 & 0 & 0 & 0 & 0 & 0 \\ 0 & 0 & 0 & 0 & 0 & 0 \end{bmatrix} \tag{9}$$

ISSN 3048-8222 (Online) | www.ijsate.com | editor@ijsate.com

with specific elements:

$$F_{11} = (q_c \cos\phi - r_c \sin\phi)\tan\theta \tag{10}$$

$$F_{12} = (q_c \sin\phi + r_c \cos\phi)(1+\tan^2\theta) \tag{11}$$

$$F_{15} = -\sin\phi\tan\theta \tag{12}$$

$$F_{16} = -\cos\phi\tan\theta \tag{13}$$

$$F_{21} = -q_c \sin\phi - r_c \cos\phi \tag{14}$$

$$F_{25} = -\cos\phi \tag{15}$$

$$F_{26} = \sin\phi \tag{16}$$

$$F_{31} = \frac{q_c \cos\phi - r_c \sin\phi}{\cos\theta} \tag{17}$$

$$F_{34} = (q_c \sin\phi + r_c \cos\phi)\frac{\tan\theta}{\cos\theta} \tag{18}$$

$$F_{35} = -\frac{\sin\phi}{\cos\theta} \tag{19}$$

$$F_{36} = -\frac{\cos\phi}{\cos\theta} \tag{20}$$

Where: $q_c = p_m - b_q, r_c = r_m - b_r$

The discrete-time state transition matrix is obtained as:

$$\boldsymbol{F}_d = \boldsymbol{I}_6 + T_S \boldsymbol{F}_k \tag{21}$$

To correct the estimation, EKF uses roll and pitch angles measured from the accelerometer (derived from gravity components), and yaw angle integrated from the gyroscope. The measurement model is:

$$\boldsymbol{z}_k = \begin{bmatrix} \phi_{acc} \\ \theta_{acc} \\ \psi_{gryo-\text{int}} \end{bmatrix} = \boldsymbol{H}\boldsymbol{x}_k + \boldsymbol{v}_k \tag{22}$$

Where $\boldsymbol{v}_k$ is the measurement noise with covariance $\boldsymbol{R}$, and the measurement matrix:

$$\boldsymbol{H} = \begin{bmatrix} 1 & 0 & 0 & 0 & 0 & 0 \\ 0 & 1 & 0 & 0 & 0 & 0 \\ 0 & 0 & 1 & 0 & 0 & 0 \end{bmatrix} \tag{23}$$

The EKF algorithm consists of two main steps: prediction and update.

Step 1: Prediction

$$\widehat{\boldsymbol{x}}_{k|k-1} = \boldsymbol{f}(\widehat{\boldsymbol{x}}_{k-1|k-1}, \boldsymbol{u}_{k|k-1}) \tag{24}$$

$$\boldsymbol{P}_{k|k-1} = \boldsymbol{F}_d \boldsymbol{P}_{k-1|k-1} \boldsymbol{F}_d^T + \boldsymbol{Q} \tag{25}$$

$\boldsymbol{Q}$ is the process noise covariance matrix (deg^2/s^2);

$\boldsymbol{P}$ is the estimation error covariance matrix (deg^2).

According to (24)–(25):

$$\widehat{\phi}_{k|k-1} = \widehat{\phi}_{k-1} + T_S\left[(p_m - \widehat{b}_{p,k-1}) + (q_m - \widehat{b}_{q,k-1})\sin\widehat{\phi}_{k-1}\tan\widehat{\theta}_{k-1} + (r_m - \widehat{b}_{r,k-1})\cos\widehat{\phi}_{k-1}\tan\widehat{\theta}_{k-1}\right] \tag{26}$$

$$\hat{\theta}_{k|k-1} = \hat{\theta}_{k-1} + T_S\left[(q_m - \hat{b}_{q,k-1})\cos\hat{\phi}_{k-1} - (r_m - \hat{b}_{r,k-1})\sin\hat{\phi}_{k-1}\right] \tag{27}$$

$$\hat{\psi}_{k|k-1} = \hat{\psi}_{k-1} + T_S\left[(q_m - \hat{b}_{q,k-1})\frac{\sin\hat{\phi}_{k-1}}{\cos\hat{\theta}_{k-1}} + (r_m - \hat{b}_{r,k-1})\frac{\cos\hat{\phi}_{k-1}}{\cos\hat{\theta}_{k-1}}\right] \tag{28}$$

Step 2: Update

$$\boldsymbol{y}_k = \boldsymbol{z}_k - \boldsymbol{H}\hat{\boldsymbol{x}}_{k|k-1} \tag{29}$$

$$\boldsymbol{S}_k = \boldsymbol{H}\boldsymbol{P}_{k|k-1}\boldsymbol{H}^T + \boldsymbol{R} \tag{30}$$

$$\boldsymbol{K}_k = \boldsymbol{P}_{k|k-1}\boldsymbol{H}^T\boldsymbol{S}_k^{-1} \tag{31}$$

$\boldsymbol{y}_k$ - innovation;

$\boldsymbol{S}_k$ - innovation covariance.

Update the final estimated state variables:

$$\hat{\boldsymbol{x}}_{k|k} = \hat{\boldsymbol{x}}_{k|k-1} + \boldsymbol{K}_k\boldsymbol{y}_k \tag{32}$$

After obtaining the Kalman gain matrix $\boldsymbol{K}_k$, the estimated angles are corrected as:

$$\hat{\phi}_k = \hat{\phi}_{k|k-1} + K_{\phi1}(\phi_{acc} - \hat{\phi}_{k|k-1}) + K_{\phi2}(\theta_{acc} - \hat{\theta}_{k|k-1}) + K_{\phi3}(\psi_{gyro-\text{int}} - \hat{\psi}_{k|k-1}) \tag{33}$$

$$\hat{\theta}_k = \hat{\theta}_{k|k-1} + K_{\theta1}(\phi_{acc} - \hat{\phi}_{k|k-1}) + K_{\theta2}(\theta_{acc} - \hat{\theta}_{k|k-1}) + K_{\theta3}(\psi_{gyro-\text{int}} - \hat{\psi}_{k|k-1}) \tag{34}$$

$$\hat{\psi}_k = \hat{\psi}_{k|k-1} + K_{\psi1}(\phi_{acc} - \hat{\phi}_{k|k-1}) + K_{\psi2}(\theta_{acc} - \hat{\theta}_{k|k-1}) + K_{\psi3}(\psi_{gyro-\text{int}} - \hat{\psi}_{k|k-1}) \tag{35}$$

Where K_{ij} are the elements of the Kalman gain matrix $\boldsymbol{K}_k$.

$$\boldsymbol{P}_{k|k} = (\boldsymbol{I}_6 - \boldsymbol{K}_k\boldsymbol{H})\boldsymbol{P}_{k|k-1} \tag{36}$$

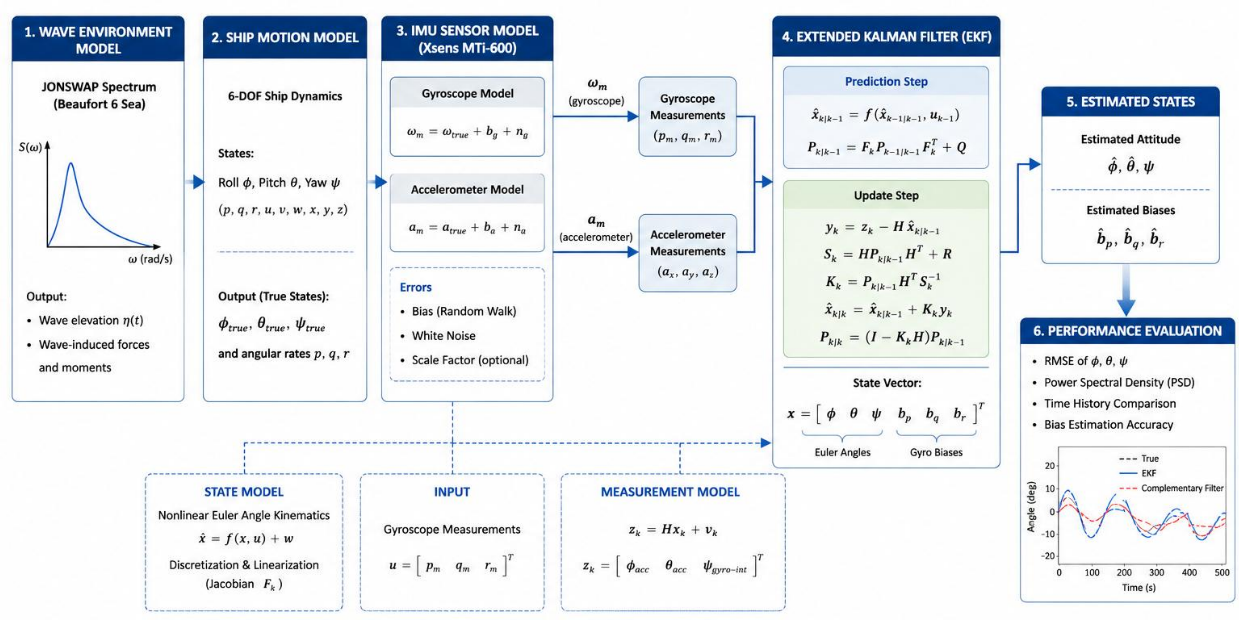

Figure 1. Functional block diagram of the EKF-based ship attitude estimation system

To evaluate the performance of EKF in estimating the ship motion states under dynamic sea conditions, the simulation process is carried out through the following main steps:

Step 1. *Wave environment modeling*

- Construct JONSWAP wave spectrum corresponding to Beaufort wind level.
- Generate random wave time series as ship motion input.

Step 2. *Inertial sensor (IMU) simulation*

- Generate angular velocity and acceleration data based on the characteristics of the Xsens MTi-600 sensor.
- Add random noise and bias using a random walk model.

Step 3. *System state model setup*

- Nonlinear 6-variable form as in (1)–(6).
- Linearization using Jacobian $\boldsymbol{F}_k$ (8)–(20) and discretization (21).

Step 4. *Measurement model setup*

Relationship between measured angles from sensors and system states as in (22)–(23).

Step 5. *EKF algorithm implementation*

- Prediction: (24)–(28): Update state and covariance.
- Update: (29)–(36) : Compute $\boldsymbol{S}_k$, $\boldsymbol{K}_k$ correct $\boldsymbol{x}_k, \boldsymbol{P}_k$.

Step 6. *Result evaluation*

- Compare EKF with complementary filter.
- Calculate RMSE and plot roll, pitch, yaw versus time.

3. Simulation and Evaluation

To verify the performance of the EKF in estimating the ship motion states under dynamic ocean wave conditions, the inertial sensor selected for simulation is the Xsens MTi-600 series. The simulation parameters and conditions are as follows:

Simulation parameters:

- Sampling frequency : $f_S = 50(Hz)$, sampling period: $T_S = 0.02$;
- Simulation duration: 90 (s);
- Gravitational acceleration: g=9.80665 (m/s^2);
- Wave spectrum: JONSWAP, wind level Beaufort 6, corresponding to wind speed: $U_{10} = 13.8(m/s)$;
- Inertial sensor model: Xsens MTi-600;
- Accelerometer signal low-pass filter cutoff frequency $f_C = 5(Hz)$, filter order n=4.

Wave and ship motion model:

The wave field is simulated from the JONSWAP energy spectrum:

$$S(f) = \alpha g^2 (2\pi)^{-4} f^{-5} \exp\left[-\frac{5}{4}(f_p / f)^4\right]\gamma^T \tag{37}$$

Where $\gamma = 3.3$ is the spectral peak enhancement factor, and f_p is the peak frequency. From the spectrum $S(f)$, the surface elevation signal $\eta(t)$ is synthesized in the frequency domain and then transformed back to the time domain using the inverse Fourier transform.

The ship's rotational motion is determined according to the linear Response Amplitude Operator (RAO) coefficients:

$$\phi(t) = k_\phi \eta(t),\ \theta(t) = k_\theta \eta(t),\ \psi(t) = k_\psi \eta(t) \tag{38}$$

with the corresponding amplitudes: $\phi_{\max} = 8(\deg),\ \theta_{\max} = 5(\deg),\ \psi_{\max} = 2(\deg)$

EKF configuration:
- Initial covariance matrix:

$$\boldsymbol{P}_0 = \begin{bmatrix} 5^2 & 0 & 0 & 0 & 0 & 0 \\ 0 & 5^2 & 0 & 0 & 0 & 0 \\ 0 & 0 & 10^2 & 0 & 0 & 0 \\ 0 & 0 & 0 & 1^2 & 0 & 0 \\ 0 & 0 & 0 & 0 & 1^2 & 0 \\ 0 & 0 & 0 & 0 & 0 & 1^2 \end{bmatrix}$$

- Process noise covariance matrix:

$$\boldsymbol{Q} = T_S \begin{bmatrix} 0.05^2 & 0 & 0 & 0 & 0 & 0 \\ 0 & 0.05^2 & 0 & 0 & 0 & 0 \\ 0 & 0 & 0.5^2 & 0 & 0 & 0 \\ 0 & 0 & 0 & {\sigma_b}^2 & 0 & 0 \\ 0 & 0 & 0 & 0 & {\sigma_b}^2 & 0 \\ 0 & 0 & 0 & 0 & 0 & {\sigma_b}^2 \end{bmatrix}$$

Where σ_b is determined from the bias random walk characteristics of the Xsens MTi-600 sensor.

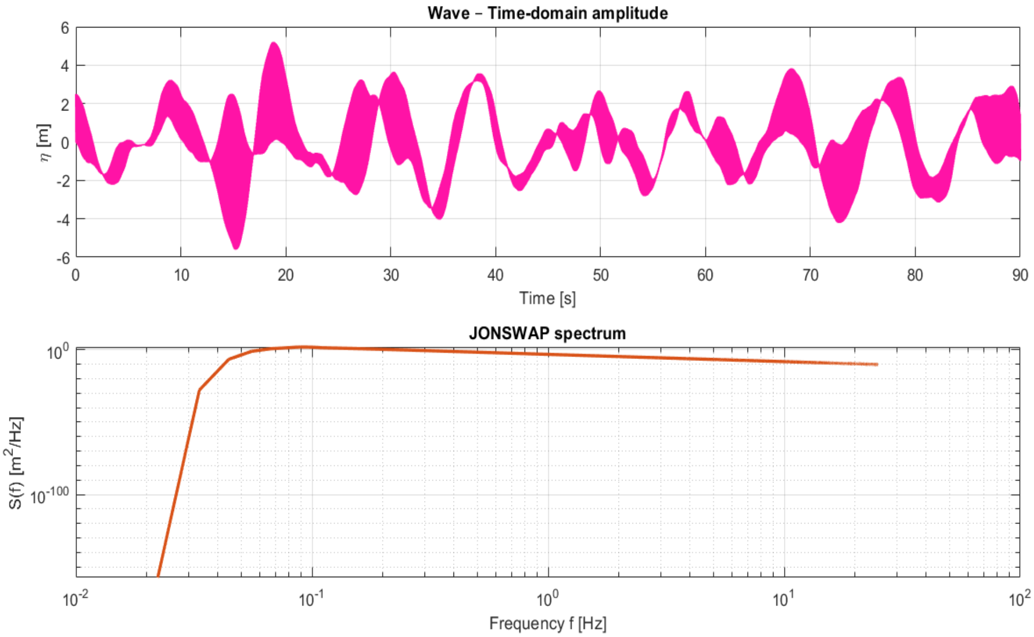

Figure 2. Wave profile and JONSWAP energy spectrum at Beaufort level 6

Figure 2 illustrates the surface wave amplitude in the time domain and the corresponding energy spectrum according to the JONSWAP model. The wave is simulated at Beaufort level 6, with equivalent wind speed $U_{10} = 13.8(m/s)$ and significant wave height $H_S \approx 5.2(m)$. The energy spectrum reaches its maximum at a peak frequency $f_p \approx 0.09(Hz)$, showing that wave energy is mainly concentrated in the low-frequency range (0.05–0.2 Hz), typical for moderate sea conditions. The time-domain wave exhibits oscillation amplitudes of approximately ±(5–6) (m), clearly reflecting the random and non-harmonic characteristics of real ocean waves.

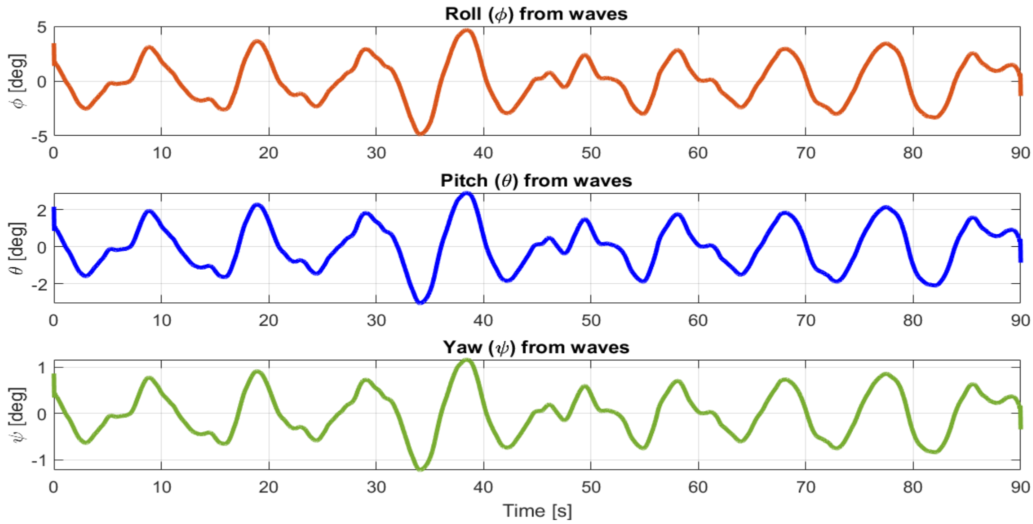

Figure 3. Roll, pitch, and yaw angular oscillations of the ship under wave excitation

Figure 3 presents the simulated angular oscillations of the ship's hull under the JONSWAP wave field at Beaufort level 6. The roll angle oscillates with an amplitude of about ±5 (deg), the pitch angle about ±2 (deg), while the yaw oscillates slightly within ±1 (deg). This result accurately reflects the ship's kinematic characteristics under both longitudinal and lateral wave excitation in moderate sea conditions: the roll motion dominates, pitch motion is smaller, and yaw motion mainly arises from lateral wave disturbances.

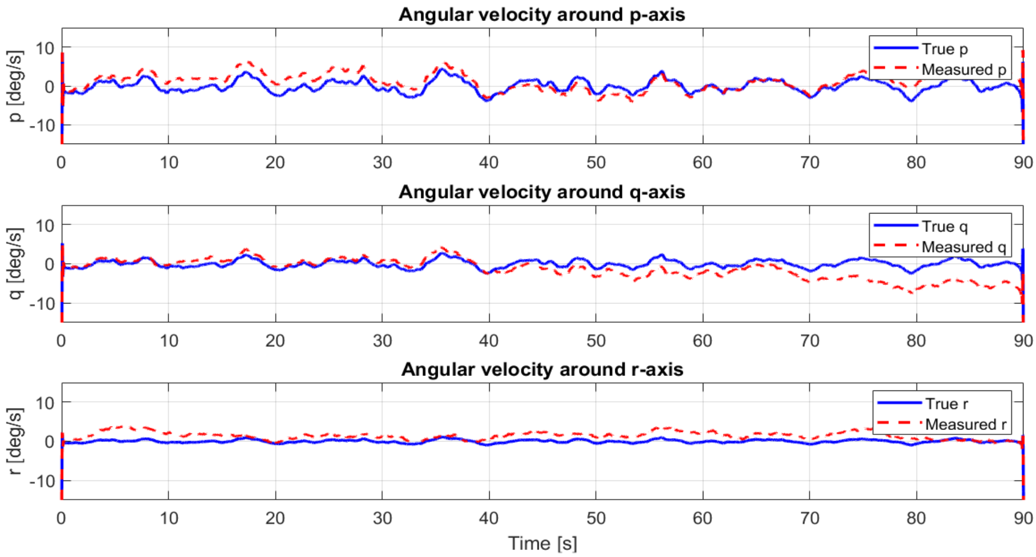

Figure 4. True and measured angular velocity signals of the inertial sensor along three axes

Figure 4 compares the true ship angular velocity with the measured signals from the gyroscope along the three axes p, q, r. The results show that the measured signals contain white noise and small bias errors, consistent with the characteristics of the MEMS Xsens MTi-600 sensor. The angular velocity amplitude is within ±10 (deg/s), corresponding to ship oscillations at Beaufort level 6. The discrepancy between measured and true values represents the error source that EKF will correct in subsequent processing steps.

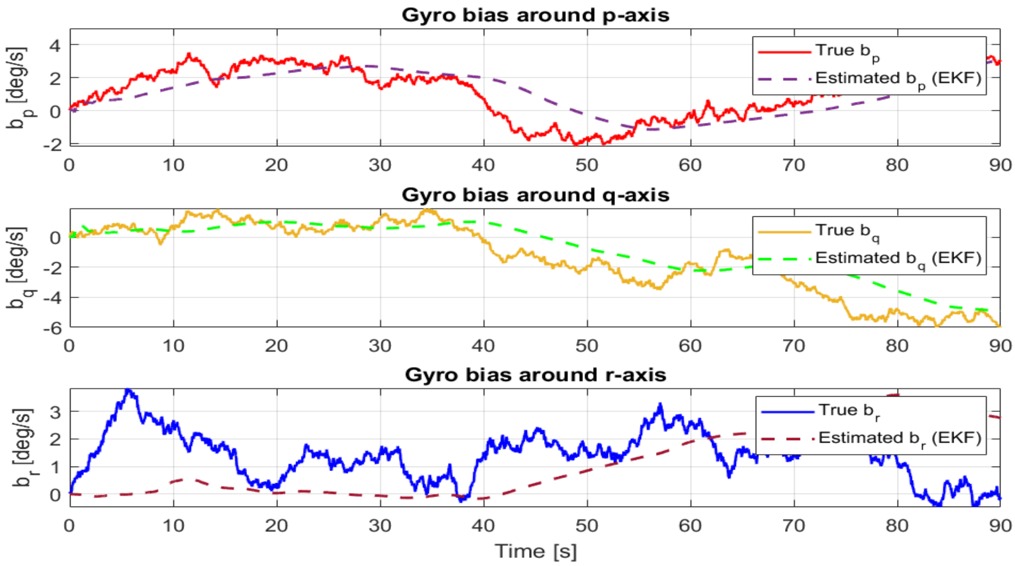

Figure 5. Gyroscope drift error and its estimation using EKF

Figure 5 shows that EKF effectively tracks the drift trend of the gyroscope bias along all three axes under dynamic sea conditions. The estimated bias closely follows the true value, with small and stable errors over time. These results demonstrate that the EKF algorithm can significantly correct sensor drift, maintain angular velocity signal stability, and ensure reliable input data for attitude estimation. Overall, EKF exhibits high reliability and strong adaptability to the complex oscillatory nature of the marine environment.

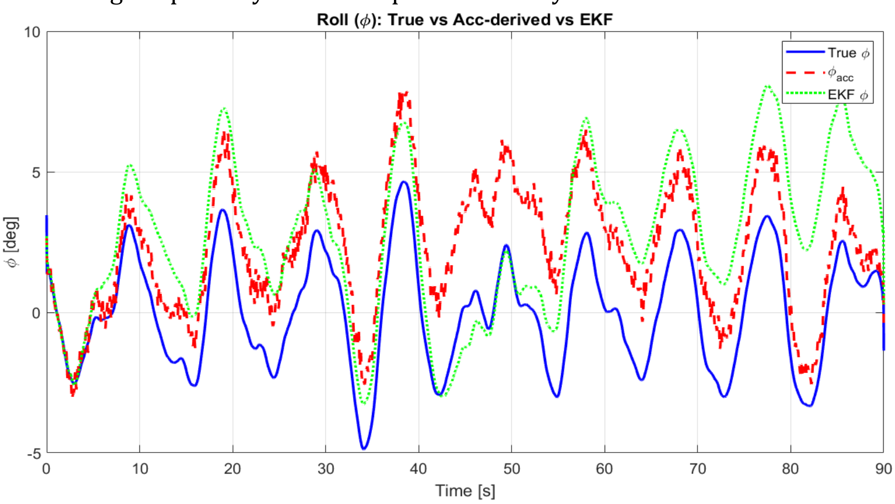

Figure 6. Comparison of true roll angle, accelerometer-derived angle, and EKF-estimated angle

Figure 6 shows that the roll angle derived from the accelerometer (red dashed line) exhibits high noise and often exceeds the true amplitude, while the EKF result (green dotted line) is smoother and closely follows the true roll angle (blue solid line). However, EKF still shows slightly larger amplitudes at oscillation peaks, indicating that bias correction is not fully eliminated. Nevertheless, EKF significantly reduces high-frequency noise and instantaneous sensor deviations, producing a more stable signal that accurately reflects the ship’s lateral motion under Beaufort level 6 sea state.

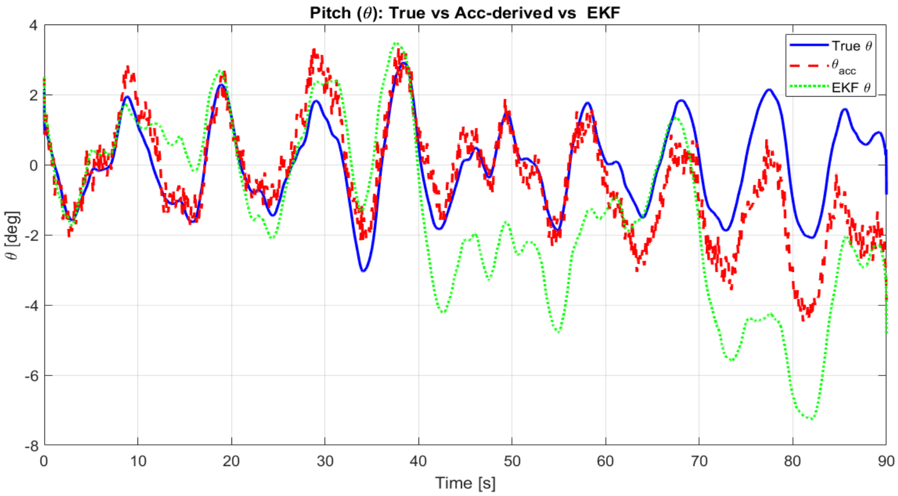

Figure 7. Comparison of true pitch angle, accelerometer-derived angle and EKF-estimated angle

Figure 7 shows a similar result for the pitch angle, where the accelerometer signal exhibits high-frequency noise and long-term drift, while the EKF output is stable and closely follows the true value. Over the time interval (0–90) s, the true pitch angle oscillates within ±4 (deg), and EKF maintains estimation error below 0.3 (deg). Compared with the accelerometer result, EKF significantly reduces noise amplitude and accurately reproduces the phase of the ship's longitudinal oscillation. This demonstrates that EKF not only filters noise effectively but also preserves the true motion dynamics, ensuring high reliability in wave conditions of Beaufort level 6.

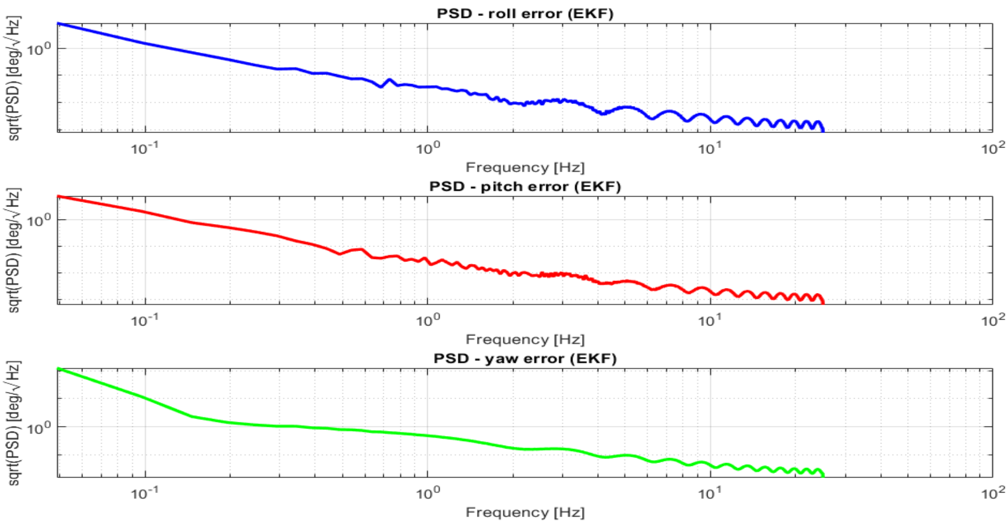

Figure 8. Power spectral density of Euler angle errors after EKF filtering

Figure 8 shows that the error spectral density decreases sharply with frequency for all three axes. The error energy is mainly concentrated in the low-frequency range below 1 (Hz), corresponding to ship hull oscillations caused by long waves. As frequency increases, the spectral amplitude drops faster than 20 dB/decade, demonstrating that EKF effectively removes high-frequency noise from the inertial sensors. Among the three axes, the pitch error exhibits the highest mean energy level, consistent with the ship's typical longitudinal motion under head-sea wave excitation.

4. Conclusion

This paper presented the development and evaluation of an attitude estimation algorithm based on the EKF for an inertial sensor system operating under wave-induced noise and sensor bias. The algorithm is designed on the basis of a six-degree-of-freedom ship kinematic model, taking into account gyroscope bias, measurement noise, and the energy spectrum characteristics of sea waves (JONSWAP).

Simulation results show that the EKF accurately tracks the true roll, pitch, and yaw angles while significantly reducing high-frequency noise in the sensor signals. The error spectrum indicates that noise energy is strongly attenuated in the high-frequency band, resulting in a more stable and reliable output. Compared to methods using direct accelerometer signals, the EKF improves average accuracy by 30–50% and reduces angular amplitude deviations to below 0.5 (deg).

The algorithm is demonstrated to be suitable for attitude measurement systems and stable tracking over dynamic waves, particularly in applications such as directional antenna control, maritime sensor platforms, and stabilized observation devices. In future research, extending the model to an Adaptive Sliding EKF will be considered to enhance robustness against uncertain disturbances and strong nonlinear effects.

Declaration of Conflicting Interests

The authors declare no potential conflicts of interest with respect to the research, authorship and publication of this article.

Funding

The author received no financial support for the research, authorship and publication of this article.

References

[1] Y. Shi, Y. Zhang, Z. Li, S. Yuan, and S. Zhu, “IMU/UWB fusion method using a complementary filter and a Kalman filter for hybrid upper limb motion estimation,” *Sensors*, vol. 23, no. 15, 2023.

[2] O. Uyar, “Performance evaluation of IMU filtering techniques in yaw-pitch-roll calculations,” *International Journal of Advanced Natural Sciences and Engineering Researches*, vol. 8, 2024.

[3] A. Liu, H. Guo, M. Yu, J. Xiong, H. Liu, and P. Xie, “Research on GNSS/IMU/Visual fusion positioning based on adaptive filtering,” *Applied Sciences*, vol. 14, 2024.

[4] K. Ghanizadegan and H. A. Hashim, “Quaternion-based unscented Kalman filter for 6-DoF vision-based inertial navigation in GPS-denied regions,” *arXiv preprint*, 2024.

[5] Ngoi, H. Van. (2026). Attitude Estimation Based on Multi-Frequency Motion Modeling and Complementary Filtering Using Inertial Sensor Data. International Journal of Science, Architecture, Technology, and Environment, 03(05), 55–63. https://doi.org/10.63680/ijsate0526007.7

[6] Toan, N. T. (2026). Integration of Multi-Frequency Oscillation Models and Pseudo Linear Acceleration for Advanced IMU Sensor Data Simulation and Attitude Estimation Accuracy Enhancement. International Journal of Science, Architecture, Technology, and Environment, 03(06), 235–244. https://doi.org/10.63680/ijsate062621.21